Satellite mapping of rain-induced nitric oxide emissions from soils

L. Jaeglé,[1] R. V. Martin,[2,3] K. Chance,[4] L. Steinberger,[1] T. P. Kurosu,[4] D. J. Jacob,[5] A. I. Modi,[6] V. Yoboué,[7] L. Sigha-Nkamdjou,[8] and C. Galy-Lacaux[9]

Received 18 March 2004; revised 16 July 2004; accepted 5 August 2004; published 12 November 2004.

[1] We use space-based observations of NO_2 columns from the Global Ozone Monitoring Experiment (GOME) to map the spatial and seasonal variations of NO_x emissions over Africa during 2000. The GOME observations show not only enhanced tropospheric NO_2 columns from biomass burning during the dry season but also comparable enhancements from soil emissions during the rainy season over the Sahel. These soil emissions occur in strong pulses lasting 1–3 weeks following the onset of rain, and affect 3 million km^2 of semiarid sub-Saharan savanna. Surface observations of NO_2 from the International Global Atmospheric Chemistry (IGAC)/Deposition of Biochemically Important Trace Species (DEBITS)/Africa (IDAF) network over West Africa provide further evidence for a strong role for microbial soil sources. By combining inverse modeling of GOME NO_2 columns with space-based observations of fires, we estimate that soils contribute 3.3 ± 1.8 TgN/year, similar to the biomass burning source (3.8 ± 2.1 TgN/year), and thus account for 40% of surface NO_x emissions over Africa. Extrapolating to all the tropics, we estimate a 7.3 TgN/year biogenic soil source, which is a factor of 2 larger compared to model-based inventories but agrees with observation-based inventories. These large soil NO_x emissions are likely to significantly contribute to the ozone enhancement originating from tropical Africa. *INDEX TERMS:* 0315 Atmospheric Composition and Structure: Biosphere/atmosphere interactions; 0322 Atmospheric Composition and Structure: Constituent sources and sinks; 0365 Atmospheric Composition and Structure: Troposphere—composition and chemistry; 1640 Global Change: Remote sensing; 3354 Meteorology and Atmospheric Dynamics: Precipitation (1854); *KEYWORDS:* soil, NO_x, satellite

Citation: Jaeglé, L., R. V. Martin, K. Chance, L. Steinberger, T. P. Kurosu, D. J. Jacob, A. I. Modi, V. Yoboué, L. Sigha-Nkamdjou, and C. Galy-Lacaux (2004), Satellite mapping of rain-induced nitric oxide emissions from soils, *J. Geophys. Res.*, *109*, D21310, doi:10.1029/2004JD004787.

1. Introduction

[2] Emissions of atmospheric nitrogen oxides (NO_x, the sum of nitric oxide and nitrogen dioxide, NO + NO_2) lead to hemispheric-scale enhancements in tropospheric ozone, rain acidification, and increased oxidizing capacity of the troposphere. In addition, through their influence on aerosol composition and on the burdens of many greenhouse gases (ozone, methane, and hydrofluorocarbons), NO_x emissions indirectly affect the Earth's radiative balance [*Prather and Ehhalt*, 2001]. Human-initiated fires are the main anthropogenic source of NO_x in tropical regions, while fossil fuel combustion dominates anthropogenic sources in Northern Hemisphere midlatitudes [*Logan*, 1983; *Penner et al.*, 1991; *Holland and Lamarque*, 1997]. Natural sources include microbial processes in soils, lightning and transport from the stratosphere.

[3] Tropical soils have been identified as significant NO_x sources, accounting for nearly 70% of global soil emissions [*Yienger and Levy*, 1995]. Many field and laboratory experiments have reported large pulses of biogenic NO emissions following rain on dry soils of savannas and seasonally dry forests [*Johansson and Sanhueza*, 1988; *Davidson*, 1992; *Harris et al.*, 1996; *Levine et al.*, 1996; *Scholes et al.*, 1997]. Long dry periods in these tropical ecosystems allow soils to accumulate inorganic nitrogen. The first rains of the wet season activate water-stressed nitrifying bacteria, leading to the consumption of accumulated nitrogen and as a by-product, to the release of large pulses of NO [*Davidson*, 1992, and references therein]. After the excess nitrogen is

[1]Department of Atmospheric Sciences, University of Washington, Seattle, Washington, USA.
[2]Department of Physics and Atmospheric Science, Dalhousie University, Halifax, Nova Scotia, Canada.
[3]Also at Harvard-Smithsonian Center for Astrophysics, Cambridge, Massachusetts, USA.
[4]Harvard-Smithsonian Center for Astrophysics, Cambridge, Massachusetts, USA.
[5]Division of Engineering and Applied Sciences and Department of Earth and Planetary Sciences, Harvard University, Cambridge, Massachusetts, USA.
[6]Département de Physique, Ecole Normale Supérieure, University Abdou Moumouny of Niamey, Niamey, Niger.
[7]Laboratoire de Physique de l'Atmosphère, Université de Cocody, Abidjan, Ivory Coast, Africa.
[8]Centre de Recherches Hydrologiques, Yaoundé, Cameroon.
[9]Observatoire Midi-Pyrénées, Laboratoire d'Aérologie, Toulouse, France.

0148-0227/04/2004JD004787

consumed, wet season NO emissions decrease but remain at relatively high levels compared to the dry season [*Serça et al.*, 1998].

[4] The inherent large spatial and temporal inhomogeneity in soil-atmospheric NO_x exchange has lead to poorly constrained estimates of its contribution to the global NO_x budget: 5–21 TgN/year (1 Tg = 10^{12}g) [*Logan*, 1983; *Davidson*, 1991; *Müller*, 1992; *Yienger and Levy*, 1995; *Potter et al.*, 1996; *Davidson and Kingerlee*, 1997]. The upper end of these estimates is comparable to global NO_x emissions from fossil fuel combustion (20–24 TgN/year). The most commonly used methods to determine these emissions are "bottom-up" approaches, which include global extrapolations of surface flux measurements [*Davidson*, 1991; *Davidson and Kingerlee*, 1997], semiempirical models [*Müller*, 1992; *Yienger and Levy*, 1995], and more complex process-based models of land-vegetation biogeochemistry [*Potter et al.*, 1996; *Parton et al.*, 2001]. Uncertainties in each of these inventories are difficult to estimate and are potentially very large (±5–10 TgN/year) [*Davidson and Kingerlee*, 1997], in part because of the role of plant canopy in recapturing soil NO_x [*Jacob and Bakwin*, 1991; *Ganzeveld et al.*, 2002].

[5] Space-based observations of NO_2 columns from the Global Ozone Monitoring Experiment (GOME) on board the European Remote Sensing (ERS-2) satellite [*Bednarz*, 1995] directly track surface NO_x emissions because of the short lifetime of NO_x (<1 day) and the high NO_2/NO_x ratio (>0.8) in the boundary layer. These observations can thus provide an independent "top-down" constraint to improve NO_x emission inventories, as recently demonstrated by *Leue et al.* [2001] and *Martin et al.* [2003].

[6] In this study, we focus on Africa during 2000 and show that remotely sensed GOME tropospheric NO_2 columns can map the elusive first-rains pulse. We partition NO_x sources between biomass burning, soils, fossil fuel combustion and domestic biomass fuel (biofuel) combustion by exploiting the spatiotemporal distribution of fires observed on the Tropical Rainfall Measuring Mission (TRMM) satellite. This allows us to quantify soil NO_x emissions and contrast them to biomass burning emissions. In addition, we use surface NO_2 observations from the International Global Atmospheric Chemistry (IGAC)/Deposition of Biochemically Important Trace Species (DEBITS)/Africa (IDAF) network of passive samplers in West Africa to support our findings.

2. Observations and Methods

2.1. Satellite Observations

[7] The GOME instrument, in a Sun-synchronous orbit aboard the ERS-2 satellite, is a nadir-viewing spectrometer with a ground footprint of 320 km (across-track) by 40 km (along-track) that achieves global coverage in 3 days. GOME measures sunlight reflected by the Earth at ultraviolet, visible and near-infrared wavelengths, thus detecting absorption of atmospheric NO_2. Slant columns of NO_2 for the year 2000 are obtained by nonlinear least squares fitting of backscattered radiance spectra over the 423–451 nm spectral region [*Chance et al.*, 2000; *Martin et al.*, 2003].

[8] Stratospheric NO_2 column and instrument biases are removed following *Martin et al.* [2002a]. The air mass factor (AMF) calculation, used to convert the tropospheric slant columns to vertical columns, accounts for scattering by the surface, clouds, aerosols and gases in the atmosphere [*Martin et al.*, 2002a, 2003]. Local cloud information is obtained from the GOME Cloud Retrieval Algorithm (GOMECAT) [*Kurosu et al.*, 1999]. The GEOS-CHEM global model of tropospheric chemistry and the GOCART global model of tropospheric aerosols (section 2.3) are used to specify the vertical shape factor of NO_2 and aerosol profiles. Of particular interest to our study is the application of the aerosol correction to the AMF calculation, as developed by *Martin et al.* [2003]. High levels of absorbing aerosols over biomass burning regions lead to a reduction of the AMF by up to 40% over the African biomass burning regions.

[9] To minimize uncertainties, all reported GOME columns are for scenes where less than 50% of backscattered radiation comes from clouds, corresponding to cloud cover <40% (unless otherwise noted). Uncertainties for each GOME scene include a 10^{15} molecules cm^{-2} absolute error from spectral fitting and removal of the stratosphere, and a 42% relative error from the AMF calculation (including errors from surface reflectivity, NO_2 profile, aerosols, cloud cover and radiative transfer). These errors result in a monthly mean tropospheric column relative uncertainty of ~30% and a 5×10^{14} molecules cm^{-2} absolute uncertainty for each 2° latitude by 2.5° longitude grid box, assuming random errors in spectral fitting, surface reflectivity and clouds.

[10] Infrared emission from fires is detected by the Visible and Infrared Scanner (VIRS) on board TRMM. We use here the monthly gridded product (0.5° × 0.5°) [*Giglio et al.*, 2003]. In addition, we use the monthly and daily TRMM precipitation products (3B43 and 3B42), which combine TRMM observations together with observations from geosynchronous infrared satellite data and rain gauge information [*Adler et al.*, 2000]. These precipitation products have been validated against a high-density rain gauge data set over West Africa and show no bias [*Nicholson et al.*, 2003]. Finally, we use lightning detected by the Lightning Imaging Sensor (LIS) on board TRMM [*Christian et al.*, 1999]. We gridded the lightning flashes on a 1° × 1° degree grid to obtain monthly and daily maps.

2.2. IDAF Surface NO_2 Observations

[11] Monthly surface measurements of NO_2 from the IDAF network in Africa (http://medias.obs-mip.fr/idaf) are obtained with passive samplers [*Galy-Lacaux et al.*, 2001]. Ambient air diffuses to a filter impregnated in an iodine salt solution, resulting in the conversion of NO_2 to NO_2^-: $2\ NO_2(g) + 3I^- \rightarrow 2\ NO_2^- + I_3^-$. The filters are exposed for one month and then are analyzed by ion chromatography. The detection limit is 0.3 ppbv and the reproducibility is 3.7%.

[12] This technique has been tested in urban, rural and remote stations [*Ferm and Rodhe*, 1997; *Ferm and Svanberg*, 1998]. The passive samplers have also been tested and validated for the IDAF network since the beginning of 1998 [*Al Ourabi and Lacaux*, 1999]. The three IDAF sites discussed here, Banizoumbou in Niger (13.3°N, 2.4°E), Lamto in Ivory Coast (6.1°N, 5.0°W) and Zoétélé in Cameroon (3.1°N, 11.6°E), are located along a transect representative of the semiarid savanna, humid savanna and forested equatorial ecosystems [*Galy-Lacaux and Modi*, 1998; *Sigha-Nkamdjou et al.*, 2003]. These sites are remote

from urban and industrial influence. We use monthly observations for 2000 as well as mean monthly observations for the 1998–2001 time period.

2.3. Global Models

[13] The GEOS-CHEM global three-dimensional model of tropospheric chemistry [*Bey et al.*, 2001] is driven by assimilated meteorological fields for 2000 from the Goddard Earth Observing System (GEOS) Global Modeling and Assimilation Office with a horizontal resolution of 2° latitude by 2.5° longitude and 30 vertical levels. Model version 5.05 (http://www-as.harvard.edu/trop/chemistry/geos) is used in our analysis.

[14] The model NO_x inventory includes emissions from fossil fuel, biofuel, biomass burning, soil, aircraft, stratosphere and lightning, as described by *Bey et al.* [2001] and *Martin et al.* [2002b]. More specifically, soil emissions are based on the *Yienger and Levy* [1995] algorithm, with an improved formulation of the canopy reduction factor [*Wang et al.*, 1998]. Our global above-canopy emission of NO_x from soils (6.3 TgN/year) is 15% higher compared to that of *Yienger and Levy* [1995]. Anthropogenic emissions are from the Global Emission Inventory Activity (GEIA) [*Benkovitz et al.*, 1996], scaled to 1998 levels. Biofuel emissions are from *Yevich and Logan* [2003]. We use interannually varying biomass burning emissions determined by satellite observations of fire counts and aerosols [*Duncan et al.*, 2003], with vegetation-specific emissions factors described in the work of *Staudt et al.* [2003]. Over Africa (south of 18°N), the GEOS-CHEM surface NO_x emissions are 5.2 TgN/year: 2.6 TgN/year from biomass burning, 1.8 TgN/year from soils, 0.49 TgN/year from fossil fuel, and 0.37 TgN/year from biofuel.

[15] The GOCART model of tropospheric aerosols [*Chin et al.*, 2002] is driven by the same meteorological fields as GEOS-CHEM (year 2000) and simulates the transport of 5 classes of aerosols: sulfate, dust, organic carbon, black carbon and sea-salt aerosols. GOCART also uses the interannually varying biomass burning inventory developed by *Duncan et al.* [2003]. These monthly mean aerosol fields are used both in the GEOS-CHEM simulation to account for the photochemical effects of aerosols, as well as in the AMF calculation to account for aerosol extinction (see section 2.1).

3. Seasonal Variations of NO_2 Over Africa

[16] GOME observations of tropospheric NO_2 columns over Africa are shown in Figure 1 (top) for January, June and August 2000. Also shown are observations of active fires, precipitation and lightning from the TRMM satellite. African fires are predominantly human-initiated through deforestation, shifting cultivation, gaming, and clearance of agricultural residue [*Crutzen and Andreae*, 1990]. These fires have a well-known seasonality [*Hao and Liu*, 1994], which corresponds to the dry (winter) seasons in each hemisphere: a northern fire belt in November–February, and a southern fire belt in June–October. Enhanced NO_2 columns ($>3 \times 10^{15}$ molecules cm^{-2}) clearly map onto these areas of intense biomass burning (Figure 1). High levels of NO_2 over the industrial Highveld region of South Africa and oil-producing Saudi Arabia and Egypt are also detected by GOME. In addition, unexpectedly large NO_2 columns ($>1–2 \times 10^{15}$ molecules cm^{-2}) are observed over 3 million km^2 of semiarid savannas in the so-called Sahel region during June, when no fires occur and no industrial emissions are expected. We will argue that this represents the first satellite evidence of microbial NO_x pulses following the onset of rainfall over vast areas of dry soils. As the heavy rainfall migrates northward in August, following the movement of the Intertropical Convergence Zone (ITCZ), these NO_2 enhancements over the Sahel region disappear.

[17] To further document these enhancements over the Sahel, we examine the temporal variations of NO_2, fires, rainfall and lightning over an area spanning from Mali to Sudan (12–16°N; 0–30°E). The high tropospheric NO_2 columns in January and February, corresponding to the fire season, are followed by lower columns in March and April (Figure 2). Mid-May marks the onset of rainfall over the southern Sahel after a 6-month dry season, and NO_2 columns begin to increase. By mid-June these first rains have wetted progressively larger areas and the NO_2 pulse reaches its maximum at 2.2×10^{15} molecules cm^{-2} (Figure 2, green shading). Assuming a NO_x atmospheric lifetime of 7 hours against oxidation, this corresponds to an average emission flux of 20 ng N $m^{-2}s^{-1}$, which is within the range of reported field measurement values (6–60 ng N $m^{-2}s^{-1}$) [*Johansson and Sanhueza*, 1988; *Davidson*, 1992; *Levine et al.*, 1996; *Scholes et al.*, 1997; *Serça et al.*, 1998]. A later pulse occurs in September (Figure 2, gray shading). This pulse appears to be triggered by the return of rain after a 2-week dry period, but it could also be related to the beginning of the burning season.

[18] Figure 3 (middle) shows a three-day composite map of GOME NO_2 columns for 10–12 June. During that time period, the pulse covers a strikingly large area of semiarid savannas, with the largest columns ($>3.5 \times 10^{15}$ molecules cm^{-2}) observed at the borders of Benin, Niger and Nigeria. The top panel of Figure 3 indicates dry soils (cumulative precipitation over last 14 days <20 mm, gray) and regions of pulsing (dry soils with rain occurring over the 7–12 June time period, diamonds). This analysis represents a first-order estimate of soil moisture, which affect soil NO_x emissions, but it is only an approximation, as it does not take into account soil properties. Pulsing regions are generally colocated with the NO_2 enhancements, with the exception of the Benin/Niger/Nigeria borders. Local differences in soil type and porosity might be causing this discrepancy, but other explanations such as local retrieval errors associated with clouds and/or aerosols are also possible.

[19] Surface observations of NO_2 from the IDAF network over West Africa provide further evidence for a large role for microbial soil emissions of NO_x (Figure 3, bottom). Both monthly observations for 2000 as well as average concentrations for the 1998–2001 time period are shown. The site in the semiarid savannas of Niger shows a maximum at the onset of the rainy season in May/June, with a secondary maximum associated with biomass burning in October/November. The first maximum is consistent with the emission of inorganic nitrogen that accumulated in soils during the dry season from traditional agricultural practices such as grazing, manure application and decom-

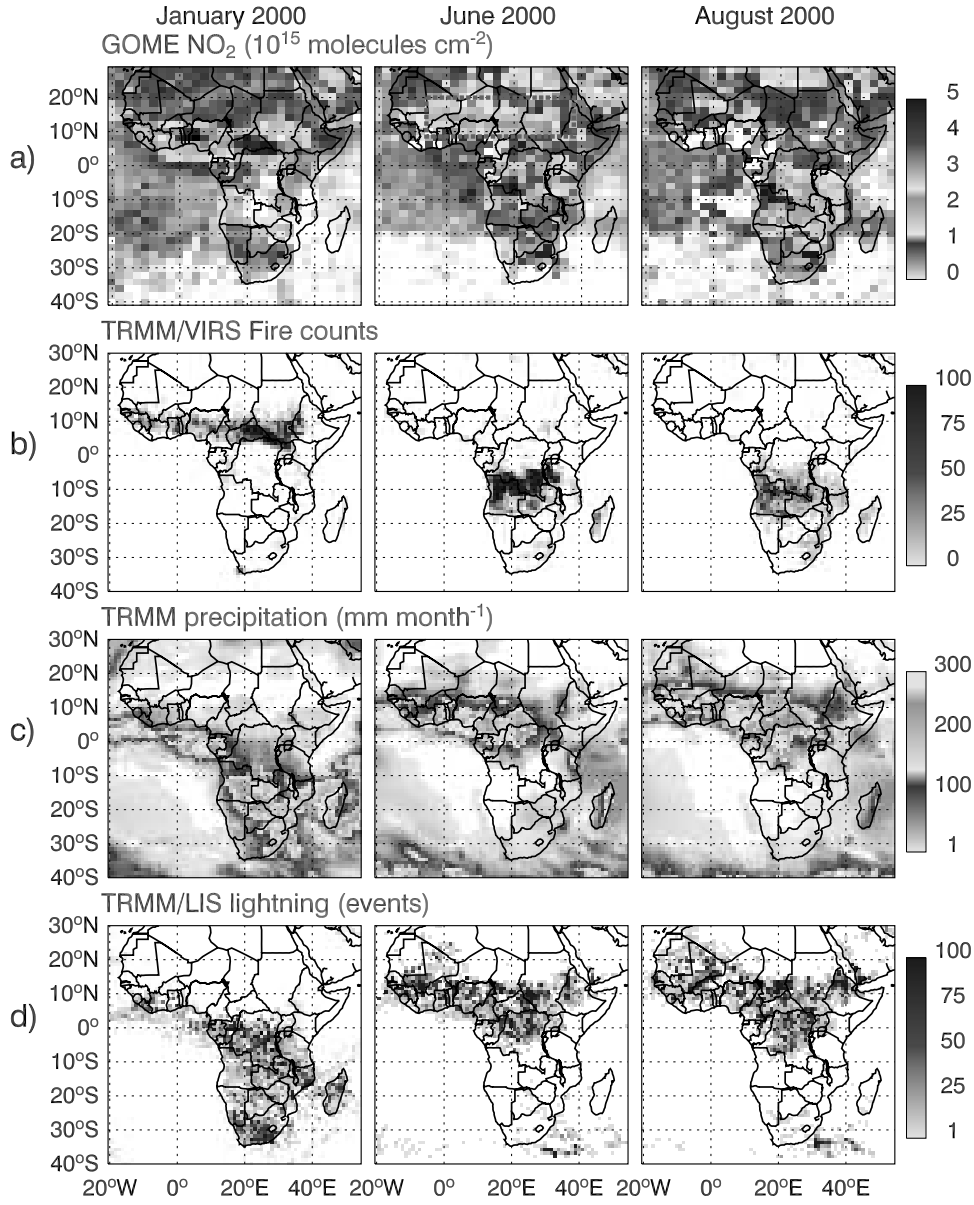

Figure 1. Space-based observations of NO_2 columns, fires, precipitation and lightning over Africa for January, June, and August 2000. (a) Monthly mean GOME NO_2 tropospheric columns in 10^{15} molecules cm^{-2}. (b) Total active fires observed by the Visible and Infrared Scanner (VIRS) on board the TRMM satellite. (c) Monthly precipitation from the TRMM merged analysis in mm $month^{-1}$. (d) Monthly lightning activity from the lightning imaging sensor (LIS) on board TRMM. GOME observations are averaged over a 2° latitude by 2.5° longitude horizontal grid, while all TRMM observations are averaged over a 1° × 1° grid. The NO_2 enhancements over the Sahel region during June are highlighted with a dotted rectangle in the top panel. See color version of this figure at back of this issue.

position of crop residues, followed by rain on the sandy soils of this area. The May/June maximum is absent from the humid ecosystems in the Ivory Coast (humid savannas) and Cameroon (tropical rain forests). This seasonality is consistent with wet season flux measurements indicating a factor of 10 difference between soil NO emissions in dry savannas compared to humid savannas [*Le Roux et al.*, 1995; *Serça et al.*, 1998]. Rainforest soils also exhibit relatively high emission rates, but most of the NO released is captured by the dense plant canopy [*Jacob and Bakwin*, 1991].

[20] Could lightning induce the remotely sensed NO_2 pulse in June? Lightning is associated with deep convective systems (and is thus related to the intensity of rainfall) but the resulting NO emissions are preferentially deposited in the upper troposphere [*Pickering et al.*, 1998]. GOME NO_2 columns are insensitive to lightning NO emissions because of the low densities and low NO_2/NO ratios in the upper troposphere [*Martin et al.*, 2003]. We use the GEOS-CHEM model to conduct a sensitivity simulation without lightning during June and find that lightning accounts for less than 0.25×10^{15} molecules cm^{-2} of NO_2 columns over the

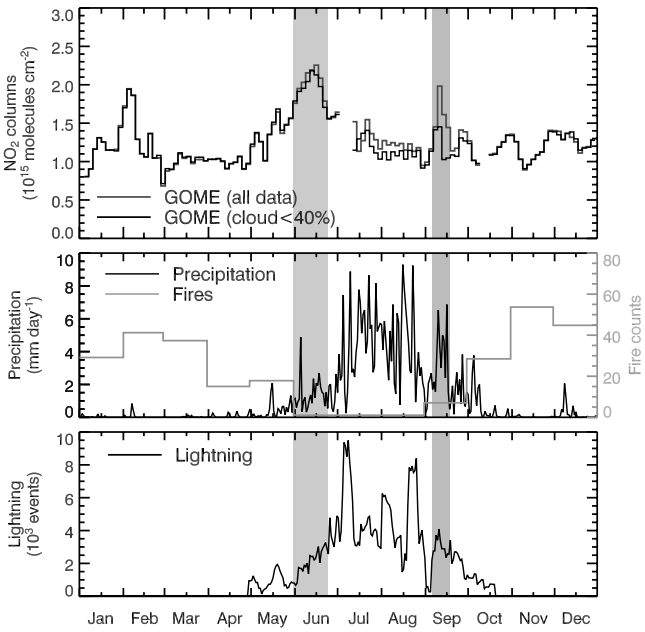

Figure 2. Evolution of NO_2, precipitation and fires over 1.5 million km^2 of the southern Sahel (12–16°N; 0–30°E). (top) Time series of 3-day composite tropospheric GOME NO_2 columns averaged over the southern Sahel. All data (red) as well as cloud-filtered data (black, <40% cloud cover) are shown. A 9-day running average was used to smooth the observations. Gaps indicate 6 days or more without observations. (middle) TRMM daily precipitation (black line) and monthly fire counts (orange line). (bottom) TRMM/LIS lightning events. The green shading indicates the June soil NO_x pulse, while the gray shading shows a later pulse in September (section 3). See color version of this figure at back of this issue.

Sahel, much less than the observed enhancement (Figure 3). Furthermore, the spatial and temporal pattern of the observed NO_2 enhancements (high over the Sahel during June and low over humid savannas and tropical rain forests) is not consistent with lightning, which maximizes over the Sahel region as well as over the Congo during July and August (Figure 1). A more detailed examination of the seasonal evolution of lightning over the Sahel (Figure 2, bottom) shows the occurrence of three local maxima in lightning (early July, early August and late August). None of these peaks is associated with an enhancement in NO_2 columns. Note that during one of these periods (early July) no GOME observations are available.

[21] Multiple scattering by clouds, which is taken into account in our retrieval, is also unlikely to contribute to the remotely sensed NO_2 pulse in June. Rainfall over Africa is generally caused by local thunderstorms and squall lines lasting a few hours and sweeping over relatively small areas. Thus while many of the 320 × 40 km^2 GOME NO_2 pixels are partially cloudy during the rainy season, cloud coverage exceeds 40% for less than half of the pixels on any given 3-day period (white pixels in Figure 3, middle). By considering only GOME scenes with less than 40% cloud coverage (black line in Figure 2, top) we find minor differences in NO_2 columns. The only notable difference is for the September pulse, which is significantly reduced in amplitude and length when we apply our cloud filter. This might indicate an underestimate of the AMF over the cloudy regions for this time period.

4. Top-Down NO_x Inventory

[22] We now relate the GOME tropospheric NO_2 column observations to surface NO_x emissions via inverse modeling with the GEOS-CHEM model. The short atmospheric lifetime of NO_x in the tropics (4–10 hours) allows direct mapping NO_2 columns, Ω_{NO2}, onto NO_x emissions, E_{NOx}, by mass balance [*Leue et al.*, 2001; *Martin et al.*, 2003] through the following linear relationship:

$$E_{NOx} = \alpha\ \Omega_{NO2} \quad (1)$$

with

$$\alpha = (\Omega_{NOx}/\Omega_{NO2})/\tau_{NOx} \quad (2)$$

where Ω_{NOx} is the tropospheric NO_x column and τ_{NOx} the NO_x lifetime against loss to stable reservoirs. We follow the methodology described by *Martin et al.* [2003] to calculate the linear coefficient α with the GEOS-CHEM model for each GOME scene ($\alpha = E_{NOx\_model}/\Omega_{NO2\_model}$). These relationships are then applied to the GOME tropospheric columns to derive top-down emissions of NO_x. To first order this method is independent of the emission inventory used in GEOS-CHEM. The primary source of uncertainty derives from the ability of the model to accurately partition between NO_x and total reactive nitrogen (NO_y). Previous comparisons of GEOS-CHEM model results with observations of the NO_x/NO_y concentration ratio over the United States [*Fiore et al.*, 2002] suggests that this source of uncertainty is less than 30%. Adding errors in quadrature, we derive an overall relative uncertainty of 42% for our top-down inventory. The absolute uncertainty of 5 × 10^{14} molecules cm^{-2} translates into a ~3 TgN/year absolute error for NO_x emissions over Africa.

[23] The resulting GOME top-down NO_x inventory is 7.8 (±4.4) TgN/year over Africa for 2000 (Table 1). The emissions are geographically distributed as follows: 4.3 TgN/year from north equatorial Africa, 3.0 TgN/year from south equatorial Africa, and 0.56 TgN/year from southern Africa. Our top-down inventory is similar to the 1997 GOME inventory presented by *Martin et al.* [2003], and is compared to the GEOS-CHEM bottom-up emission inventory in Table 1 (numbers in parenthesis). We find that it is 30–80% larger than the GEOS-CHEM inventory, with the largest discrepancy over north equatorial Africa. This discrepancy is due to model underestimates of biomass burning and soil sources, as discussed below.

5. Source Partitioning of NO_x Emissions

[24] On the basis of the GEOS-CHEM bottom-up inventory, fossil fuel and biofuel emissions account for ~0.8 TgN/year over Africa (see section 2.3). We subtract these spatially distributed bottom-up estimates (fossil + biofuels) from our GOME top-down NO_x inventory for each month. We then infer the partitioning of the residual GOME NO_x sources between biomass burning and soil

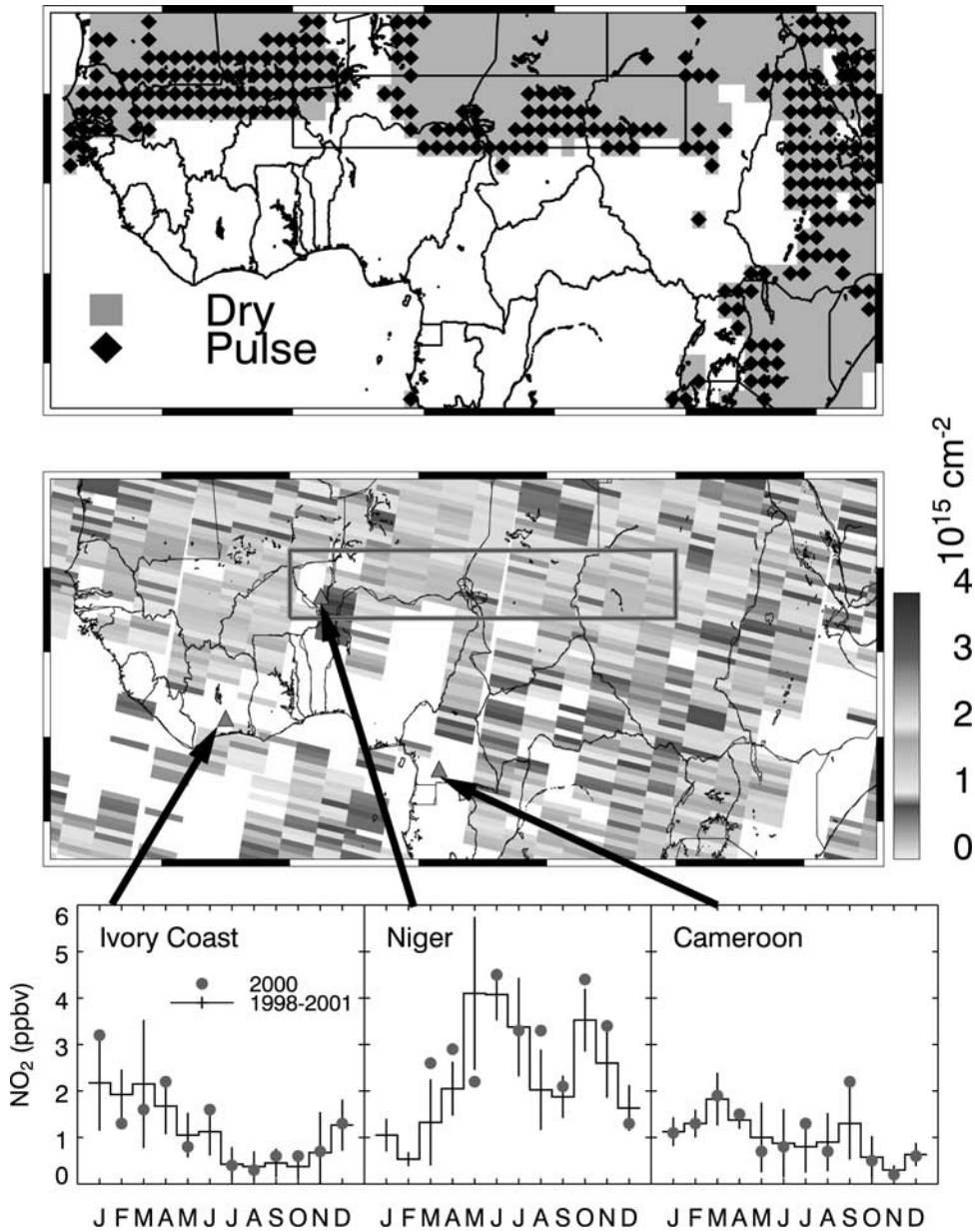

Figure 3. (top) Accumulated rainfall and soil pulsing derived from TRMM daily precipitation for 7–12 June 2000. Gray areas indicate dry soils (accumulated precipitation over the last 14 days <20 mm) and black diamonds correspond to dry soils with recent rainfall occurring over the 7–12 June time period. (middle) Three-day composite map of GOME tropospheric NO_2 columns for 10–12 June 2000. White areas are for cloud cover >40%. The thick rectangle shows the area plotted in Figure 2 (12–16°N; 0–30°E). (bottom) Monthly surface NO_2 measurements from the IDAF network in wet savanna (Lamto, Ivory Coast: 6.1°N, 5.0°W), semiarid savanna (Banizoumbou, Niger: 13.3°N, 2.4°E), and rain forest (Zoétélé, Cameroon: 3.1°N, 11.6°E) sites. Red circles show the 2000 observations, while black lines show the mean (and standard deviations) for 1998–2001. See color version of this figure at back of this issue.

Table 1. GOME Surface NO_x Emissions (Tg N/year) Over Africa in 2000[a]

	North Equatorial Africa (18°–0°N)	South Equatorial Africa (0°–24°S)	South Africa (24°–35°S)	Africa (18°N–35°S)
Fossil and biofuels	0.4 (0.4)	0.2 (0.2)	0.2 (0.2)	0.8 (0.8)
Biomass burning	1.7 (0.8)[b]	2.0 (1.8)	0.05 (0.03)	3.8 (2.6)
Soils	2.2 (1.1)	0.9 (0.5)	0.26 (0.08)	3.3 (1.7)
Total	4.3 (2.3)	3.0 (2.5)	0.56 (0.38)	7.8 (5.2)

[a]The partitioning of the GOME top-down inventory between biomass burning, soils and biofuel and fossil fuel emissions is inferred from our bottom-up biofuel and fossil fuel inventory combined with the spatial distribution of TRMM/VIRS fires on a monthly basis.
[b]The numbers in parentheses are the bottom-up emissions of NO_x from the GEOS-CHEM inventory.

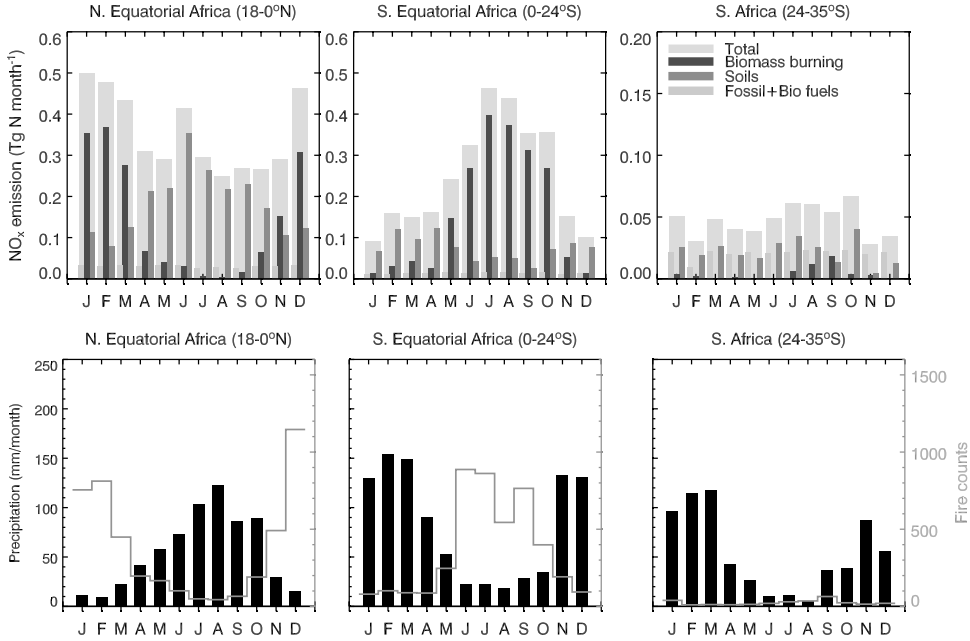

Figure 4. Monthly NO_x emissions, fires and rainfall over north equatorial Africa (18–0°N), south equatorial Africa (0–24°S) and southern Africa (24–35°S) in 2000. (top) Monthly top-down GOME NO_x emissions averaged over each region (gray bars). Note the different scale on the right-most panel. We combine bottom-up estimates of biofuel and fossil fuel NO_x emission inventories with the spatial location of fires to partition emissions between biomass burning (red bars), soil (blue bars), and fossil+biofuel (green bars) sources. (bottom) Seasonal variations in total active fires (solid orange line) and mean precipitation (black bars) observed by TRMM. See color version of this figure at back of this issue.

sources from the spatial location of fires. For each month and each $2° \times 2.5°$ grid box where at least 20 fire counts are detected we assume that all NO_x emissions are associated with biomass burning. This method is likely to lead to an upper estimate of biomass burning emissions as some non-burning sources are expected to be present even when there are fires. The use of other remotely sensed fire data sets (Along Track Scanning Radiometer (ATSR) sensor on board the ERS-2 satellite, and Global Burned Area product from the SPOT-VEGETATION instrument) does not affect our partitioning by more than 10% as we are only using the spatial distribution of fires, not their intensity.

[25] The biomass burning component of the GOME NO_x emissions is 40% for north equatorial Africa, 60% for south equatorial Africa, and 10% for southern Africa (Table 1). The total contribution from biomass burning over Africa is 3.8 (±2.1) TgN/year, within the range of previous estimates (2.8–5 TgN/year) [*Scholes and Andreae*, 2000; *Hoelzemann et al.*, 2004]. Our top-down GOME inventory agrees with the GEOS-CHEM inventory over south equatorial Africa, but is a factor of two higher over north equatorial Africa. As noted by *Martin et al.* [2003], this is likely a result of an underestimate of the NO emission factor (EF) used in our inventory for north African savannas (EF = 1.1 gNO/kg dry matter) [*Staudt et al.*, 2003]. This emission factor was based on fields measurements obtained in the wet savannas of the Ivory coast [*Lacaux et al.*, 1996], which might not be representative of dry savanna burning. Increasing the emission factor closer to values observed in South African savannas (3.9 g/kg) [*Andreae and Merlet*, 2001] would bring the two emission inventories into better agreement over north equatorial Africa.

[26] Figure 4 illustrates the seasonal variation of emissions and their partitioning between burning, soils, fossil fuel and biofuel sources. For southern Africa, the lack of seasonal variability and low contribution from burning reflect NO_x emissions dominated by year-round sources from coal combustion in households and in electricity power stations of the densely populated Mpumalanga Highveld. Over equatorial Africa, biomass burning emissions (red bars in Figure 4) control the much stronger seasonal variability during the fire season for November-March in the Northern Hemisphere and May-October in the Southern Hemisphere. Soil emissions (blue bars) also show a marked seasonal variation, with a three-fold increase between the dry and wet seasons for equatorial Africa. In fact, during June over north equatorial Africa, NO_x emissions from soil pulsing (0.4 Tg N) match those observed in February, at the height of the fire season.

[27] Fossil and biofuel emissions make only minor contributions to the total surface NO_x sources over equatorial Africa (~7%). They play a larger role over southern Africa, where our bottom-up estimates for fossil and biofuel emissions are likely too low by 25–35% over the industrial Highveld region of South Africa [*Martin et al.*, 2003].

[28] We calculate the contribution of soil emissions to the NO_x budget over Africa: 2.2, 0.9, 0.2 TgN/year for north equatorial, south equatorial, and southern Africa respectively. The large soil emissions over north equatorial Africa are consistent with the surface area of semiarid grasslands being 2.5 times larger than in south equatorial

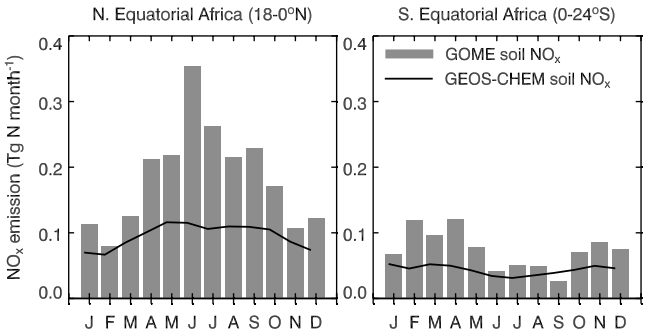

Figure 5. Seasonal variation in soil NO_x emissions for north equatorial Africa (18–0°N) and south equatorial Africa (0–24°S) in 2000. The gray bars show the monthly top-down GOME soil NO_x emissions. The solid line represents the GEOS-CHEM soil emission inventory based on Yienger and Levy.

Africa. Our top-down soil emissions over southern Africa are likely to be too high because of the underestimate of fossil and biofuel emissions noted above. Overall, soil emissions (3.3 ± 1.8 TgN/year) account for 40% of surface NO_x emissions over Africa.

[29] Extrapolating to all the tropics (Africa represents ~40% of tropical soils), we estimate a 7.3 TgN/year biogenic soil source that is consistent with the experimentally based inventory of *Davidson and Kingerlee* [1997] (7.9 TgN/year), but is a factor of two larger than the semiempirical model of *Yienger and Levy* [1995] (3.65 TgN/year) and process-based model of *Potter et al.* [1996] (3.45 TgN/year). These numbers include the Yienger and Levy canopy reduction and were obtained by adding the tropical grassland, tropical woodland, dry forest, rain forest and tropical agriculture categories listed by these authors.

[30] The two-fold difference between model-based and observation-based inventories could be due to the failure of the models to adequately account for rain-induced pulsing [*Davidson and Kingerlee*, 1997]. The *Potter et al.* [1996] model, which computes NO_x emissions from first principles, uses monthly time steps and does not have pulsing. The Yienger and Levy algorithm does include a pulsing parameterization, but could be underestimating its magnitude [*Hutchinson et al.*, 1997]. This is supported by Figure 5, which shows a direct comparison between the monthly GOME top-down soil NO_x emissions and the soils emissions computed in GEOS-CHEM using the Yienger and Levy algorithm. While both inventories agree during the dry season, there is a factor of 3 difference in the amplitude of the seasonal cycle during the wet season in both hemispheres.

[31] Most current chemical transport models are using the Yienger and Levy algorithm for soil NO_x emissions, and are thus likely to underestimate the role of these emissions in affecting tropical ozone concentrations. For example, recent studies by *Marufu et al.* [2000] and *Lelieveld and Dentener* [2000] found a 10–12% contribution of soil NO_x emissions to the tropospheric ozone column above Africa.

[32] On the basis of our GOME top-down inventory, we expect the largest influence of soil NO_x emissions on tropospheric ozone to be over and downwind of West Africa in June-August. Indeed, satellite tropospheric ozone columns (TOC) observations during that time period show a broad maximum over the Atlantic spanning from 10°N to 20°S [e.g., *Fishman and Brackett*, 1997; *Ziemke and Chandra*, 1999]. While many features in tropical TOC observations have been accounted for by contributions from biomass burning, dynamics, and lightning [e.g., *Thompson et al.*, 1996; *Jacob et al.*, 1996; *Marufu et al.*, 2000; *Moxim and Levy*, 2000; *Chandra et al.*, 2002; *Martin et al.*, 2002b], the role of soils is likely underestimated. The large soil source inferred from GOME observations suggests that soil pulsing over north equatorial Africa may play a significant role in seasonal ozone production. In addition, soils emissions in south equatorial Africa at the onset of the rainy season could help prolong the effects of fires on TOC [*Swap et al.*, 2003].

6. Conclusions

[33] We have retrieved tropospheric NO_2 columns from the Global Ozone Monitoring Experiment (GOME) over Africa for January-December 2000. The seasonal variations in tropospheric NO_2 columns track NO_x emissions from fires during the dry season. NO_2 columns are also enhanced over 3 million km^2 of the southern Sahel in June when no fires are expected. June marks the beginning of rainfall over this region, as remotely sensed by the Tropical Rainfall Measuring Mission (TRMM). We argue that these NO_2 enhancements are due to rain-induced pulsing from soils over vast areas of the Sahel.

[34] The spatial and temporal distribution of the GOME NO_2 enhancements at the beginning of the rainy season is consistent with soil NO emissions from ecosystem-dependent flux measurements and from surface measurements of NO_2 obtained by the IDAF (IGAC/DEBITS/Africa) network over West Africa. Lightning and clouds are unlikely to account for the enhanced GOME NO_2 columns and IDAF surface NO_2 observations.

[35] We have quantified the magnitude of the soil NO_x source in a two-step approach. We first related the GOME tropospheric NO_2 column observations to surface NO_x emissions via inverse modeling with the GEOS-CHEM global model of tropospheric chemistry, thus deriving a top-down emission inventory. We then inferred the monthly partitioning of NO_x sources between biomass burning, soil, and combustion of fossil or domestic biomass fuels by combining bottom-up estimates of fossil and biofuel emissions together with the spatial location of fires from the Visible and Infrared Scanner (VIRS) on board TRMM.

[36] We find a large role for soil NO_x sources over Africa, contributing 3.3 TgN/year (40% of African emissions). These emissions are similar to the biomass burning source (3.8 TgN/year). Soil emissions over north equatorial Africa (2.2 TgN/year) account for almost 70% of African soil emissions, because of the vast areas covered by dry ecosystems. By extrapolating to all the tropics, we find our estimates of soil emissions (7.3 TgN/year) to be consistent with observationally based inventories, but a factor of two higher than model-based inventories. The spatial and temporal constraints on soil NO_x emissions obtained from GOME could thus help resolve the twofold discrepancy between models and observations. Furthermore, we suggest

that rain-induced microbial pulsing over north equatorial Africa likely contributes to seasonal ozone production over and downwind of West Africa.

[37] A significant fraction of soil NO_x emissions may be driven by human perturbations such as fertilizer use, burning of vegetation and deforestation [*Keller et al.*, 1993; *Levine et al.*, 1996; *Sanhueza*, 1997]. These land use practices are likely to increase in the future, and thus continued monitoring of tropical NO_2 by satellite might help to quantify human influence on microbial soil emissions.

[38] **Acknowledgments.** We thank Mian Chin for providing the GOCART model results for 2000. This work was supported by funding from the NASA New Investigator Program in Earth Science to L.J. and by funding from NASA's Radiation Science Program to R.M. The GEOS-CHEM model is managed by the Atmospheric Chemistry Modeling group at Harvard University with support from the NASA Atmospheric Chemistry Modeling and Analysis Program.

References

Adler, R. F., G. J. Huffman, D. T. Bolvin, S. Curtis, and E. J. Nelkin (2000), Tropical rainfall distributions determined using TRMM combined with other satellite and rain gauge information, *J. Appl. Meteorol.*, *39*, 2007–2023.

Al Ourabi, H., and J. P. Lacaux (1999), Measurements of NH_3, NO_2 and HNO_3 in tropical Africa by use of diffusion samplers, paper presented at International Global Atmospheric Chemistry (IGAC) Symposium, Bologna, Italy, Sept.

Andreae, M. O., and P. Merlet (2001), Emission of trace gases and aerosols from biomass burning, *Global Biogeochem. Cycles*, *15*, 955–966.

Bednarz, F. (Ed.) (1995), ESA, in *The GOME Users Manual*, *Eur. Space Ag. Publ. SP-1182*, ESA Publ., Noordwijk.

Benkovitz, C. M., M. T. Scholtz, J. Pacyna, L. Tarrason, J. Dignon, E. C. Voldner, P. A. Spiro, J. A. Logan, and T. E. Graedel (1996), Global gridded inventories of anthropogenic emissions of sulfur and nitrogen, *J. Geophys. Res.*, *101*, 29,239–29,253.

Bey, I., D. J. Jacob, R. M. Yantosca, J. A. Logan, B. D. Field, A. M. Fiore, Q. Li, H. Y. Liu, L. J. Mickley, and M. G. Schultz (2001), Global modeling of tropospheric chemistry with assimilated meteorology: Model description and evaluation, *J. Geophys. Res.*, *106*, 23,073–23,095.

Chance, K., P. I. Palmer, R. J. D. Spurr, R. V. Martin, T. Kurosu, and D. J. Jacob (2000), Satellite observations of formaldehyde over North America from GOME, *Geophys. Res. Lett.*, *27*, 3461–3464.

Chandra, S., J. R. Ziemke, P. K. Bhartia, and R. V. Martin (2002), Tropical tropospheric ozone: Implications for dynamics and biomass burning, *J. Geophys. Res.*, *107*(D14), 4188, doi:10.1029/2001JD000447.

Chin, M., P. Ginoux, S. Kinne, O. Torres, B. N. Holben, B. N. Duncan, R. V. Martin, J. A. Logan, A. Higurashi, and T. Nakajima (2002), Tropospheric aerosol optical thickness from the GOCART model and comparisons with satellite and Sun photometer measurements, *J. Atmos. Sci.*, *59*, 461–483.

Christian, H. J., et al. (1999), The lightning imaging sensor, in *Proceedings of the 11th International Conference on Atmospheric Electricity, Guntersville, Alabama, June 7–11*, edited by H. J. Christian, pp. 746–749, NASA, Greenbelt, Md.

Crutzen, P. J., and M. O. Andreae (1990), Biomass burning in the tropics: Impact on atmospheric chemistry and biogeochemical cycles, *Science*, *250*, 1669–1678.

Davidson, E. A. (1991), Fluxes of nitrous oxide and nitric oxide from terrestrial ecosystems, in *Microbial Production and Consumption of Greenhouse Gases: Methane, Nitrogen oxides, and Halomethanes*, edited by J. E. Rogers and W. B. Whitman, pp. 219–235, Am. Soc. for Microbiol., Washington, D. C.

Davidson, E. A. (1992), Pulses of nitric oxide and nitrous oxide flux following wetting of dry soil: An assessment of probable sources and importance relative to annual fluxes, *Ecol. Bull.*, *42*, 149–155.

Davidson, E. A., and W. Kingerlee (1997), A global inventory of nitric oxide emissions from soils, *Nut. Cycl. Agroecosys.*, *48*, 37–50.

Duncan, B. N., R. V. Martin, A. C. Staudt, R. Yevich, and J. A. Logan (2003), Interannual and seasonal variability of biomass burning emissions constrained by satellite observations, *J. Geophys. Res.*, *108*(D2), 4100, doi:10.1029/2002JD002378.

Ferm, M., and H. Rodhe (1997), Measurements of air concentrations of SO_2, NO_2 and NH_3 at rural and remote sites in Asia, *J. Atmos. Chem.*, *27*, 17–29.

Ferm, M., and P. A. Svanberg (1998), Cost efficient techniques for urban and background measurements of SO_2 and NO_2, *Atmos. Environ.*, *32*, 1377–1381.

Fiore, A. M., D. J. Jacob, I. Bey, R. M. Yantosca, B. D. Field, A. C. Fusco, and J. G. Wilkinson (2002), Background ozone over the United States in summer: Origin, trend, and contribution to pollution episodes, *J. Geophys. Res.*, *107*(D15), 4275, doi:10.1029/2001JD000982.

Fishman, J., and V. G. Brackett (1997), The climatological distribution of tropospheric ozone derived from satellite measurements using Version 7 TOMS and SAGE data sets, *J. Geophys. Res.*, *102*, 19,275–19,278.

Galy-Lacaux, C., and A. I. Modi (1998), Precipitation chemistry in the Sahelian savanna of Niger, Africa, *J. Atmos. Chem.*, *30*, 319–343.

Galy-Lacaux, C., G. R. Carmichael, C. H. Song, J. P. Lacaux, H. Al Ourabi, and A. I. Modi (2001), Heterogeneous processes involving nitrogenous compounds and Saharan dust inferred from measurements and model calculations, *J. Geophys. Res.*, *106*, 12,559–12,578.

Ganzeveld, L. N., J. Lelieveld, F. J. Dentener, M. C. Krol, A. J. Bouwman, and G.-J. Roelofs (2002), Global soil-biogenic NO_x emissions and the role of canopy processes, *J. Geophys. Res.*, *107*(D16), 4298, doi:10.1029/2001JD001289.

Giglio, L., J. D. Kendall, and R. Mack (2003), A multi-year active fire dataset for the tropics derived from the TRMM VIRS, *Int. J. Remote Sensing.*, *24*, 4505–4525.

Hao, W. M., and M.-H. Liu (1994), Spatial and temporal distribution of tropical biomass burning, *Global Biogeochem. Cycles*, *8*, 495–503.

Harris, G. W., F. G. Wienhold, and T. Zenker (1996), Airborne observations of strong biogenic NO_x emissions from the Namibian savanna at the end of the dry season, *J. Geophys. Res.*, *101*, 23,707–23,711.

Hoelzemann, J. J., M. G. Schultz, G. P. Brasseur, C. Granier, and M. Simon (2004), Global Wildland Fire Emission Model (GWEM): Evaluating the use of global area burnt satellite data, *J. Geophys. Res.*, *109*, D14S04, doi:10.1029/2003JD003666.

Holland, E. A., and J.-F. Lamarque (1997), Modeling of bio-atmospheric coupling of the nitrogen cycle through NO_x emissions and NO_y deposition, *Nut. Cycl. Agroecosys.*, *48*, 7–24.

Hutchinson, G. L., M. F. Vigil, J. W. Doran, and A. Kessavalou (1997), Coarse-scale soil-atmosphere NO_x exchange modeling: Status and limitations, *Nut. Cycl. Agroecosys.*, *48*, 25–35.

Jacob, D. J., and P. S. Bakwin (1991), Cycling of NO_x in tropical forest canopies, in *Microbial Production and Consumption of Greenhouse Gases: Methane, Nitrogen Oxides, and Halomethanes*, edited by J. E. Rogers and W. B. Whitman, chap. 13, pp. 237–253, Am. Soc. for Microbiol., Washington, D. C.

Jacob, D. J., et al. (1996), Origin of ozone and NOx in the tropical troposphere: A photochemical analysis of aircraft observations over the South Atlantic basin, *J. Geophys. Res.*, *101*, 24,235–24,250.

Johansson, C., and E. Sanhueza (1988), Emissions of NO from savanna soils during the rainy season, *J. Geophys. Res.*, *93*, 14,193–14,198.

Keller, M., E. Veldkamp, A. M. Weitz, and W. A. Reiners (1993), Effect of pasture age on soil trace-gas emissions from a deforested area of Costa Rica, *Nature*, *365*, 244–246.

Kurosu, T. P., K. Chance, and R. J. D. Spurr (1999), CRAG-cloud retrieval algorithm for ESA's global ozone monitoring experiment, *Rep. ESA WPP-161*, pp. 513–521, Eur. Space Res. and Tech Cent., Noordwijk.

Lacaux, J. P., R. Delmas, C. Jambert, and T. A. J. Kuhlbusch (1996), NO_x emissions from African savanna fires, *J. Geophys. Res.*, *101*, 23,585–23,595.

Lelieveld, J., and F. J. Dentener (2000), What controls tropospheric ozone?, *J. Geophys. Res.*, *105*, 3531–3551.

Le Roux, X., L. Abbadie, R. Lensi, and D. Serça (1995), Emission of nitrogen monoxide from African tropical ecosystems: Control of emissions by soil characteristics in humid and dry savannas of West Africa, *J. Geophys. Res.*, *100*, 23,133–23,142.

Leue, C., M. Wenig, T. Wagner, O. Klimm, U. Platt, and B. Jahne (2001), Quantitative analysis of NO_x emissions from GOME satellite image sequences, *J. Geophys. Res.*, *106*, 5493–5505.

Levine, J. S., E. L. Winstead, D. A. B. Parsons, M. C. Scholes, R. J. Scholes, W. R. Cofer, D. R. Cahoon, and D. I. Sebacher (1996), Biogenic soil emissions of nitric oxide (NO) and nitrous oxide (N_2O) from savannas in South Africa: The impact of wetting and burning, *J. Geophys. Res.*, *101*, 23,689–23,697.

Logan, J. A. (1983), Nitrogen oxides in the troposphere: Global and regional budgets, *J. Geophys. Res.*, *88*, 785–807.

Martin, R. V., et al. (2002a), An improved retrieval of tropospheric nitrogen dioxide from GOME, *J. Geophys. Res.*, *107*(D20), 4437, doi:10.1029/2001JD001027.

Martin, R. V., et al. (2002b), Interpretation of TOMS observations of tropical tropospheric ozone with a global model and in situ observations, *J. Geophys. Res.*, *107*(D18), 4351, doi:10.1029/2001JD001480.

Martin, R. V., D. J. Jacob, K. Chance, T. P. Kurosu, P. I. Palmer, and M. J. Evans (2003), Global inventory of nitrogen oxide emissions constrained by space-based observations of NO_2 columns, *J. Geophys. Res.*, *108*(D17), 4537, doi:10.1029/2003JD003453.

Marufu, L., F. Dentener, J. Lelieveld, M. O. Andreae, and G. Helas (2000), Photochemistry of the African troposphere: Influence of biomass burning emissions, *J. Geophys. Res.*, *105*, 14,513–14,530.

Moxim, W. J., and H. Levy II (2000), A model analysis of tropical South Atlantic Ocean tropospheric ozone maximum: The interaction of transport and chemistry, *J. Geophys. Res.*, *105*, 17,393–17,415.

Müller, J.-F. (1992), Geographical distribution and seasonal variation of surface emissions and deposition velocities of atmospheric trace gases, *J. Geophys. Res.*, *97*, 3787–3804.

Nicholson, S. E., et al. (2003), Validation of TRMM and other rainfall estimates with a high-density gauge dataset for West Africa. Part II: Validation of TRMM rainfall products, *J. Appl. Meteorol.*, *42*, 1355–1368.

Parton, W. J., E. Holland, S. Del Grosso, M. D. Hartman, R. E. Martin, A. R. Mosier, D. S. Ojima, and D. S. Schimel (2001), Generalized model for NO_x and N_2O emissions from soils, *J. Geophys. Res.*, *106*, 17,403–17,419.

Penner, J. E., C. S. Atherton, J. Dignon, S. J. Ghan, J. J. Walton, and S. Hameed (1991), Tropospheric nitrogen: A three-dimensional study of sources, distributions, and deposition, *J. Geophys. Res.*, *96*, 959–990.

Pickering, K. E., Y. S. Wang, W. K. Tao, C. Price, and J. F. Muller (1998), Vertical distributions of lightning NO_x for use in regional and global chemical transport models, *J. Geophys. Res.*, *103*, 31,203–31,216.

Potter, C. S., P. A. Matson, P. M. Vitousek, and E. A. Davidson (1996), Process modeling of controls on nitrogen tracer gas emissions from soils worldwide, *J. Geophys. Res.*, *101*, 1361–1377.

Prather, M. J., and D. Ehhalt (2001), Atmospheric chemistry and greenhouse gases, in *Climate Change 2001: The Science of Climate Change*, chap. 4, pp. 239–287, Cambridge Univ. Press, New York.

Sanhueza, E. (1997), Impact of human activity on NO soil fluxes, *Nutr. Cycl. Agroecosys.*, *48*, 61–68.

Scholes, M., and M. O. Andreae (2000), Biogenic and pyrogenic emissions from Africa and their impact on the global atmosphere, *Ambio*, *29*, 23–29.

Scholes, M., R. Martin, R. J. Scholes, D. Parsons, and E. Winstead (1997), NO and N_2O emissions from savanna soils following the first simulated rains of the season, *Nutr. Cycl. Agroecosys.*, *48*, 115–122.

Serça, D., R. Delmas, X. Le Roux, D. A. B. Parsons, M. C. Scholes, L. Abbadie, R. Lensi, O. Ronce, and L. Labroue (1998), Comparison of nitrogen monoxide emissions from several African tropical ecosystems and influence of season and fire, *Global Biogeochem. Cycles*, *12*, 637–651.

Sigha-Nkamdjou, L., C. Galy-Lacaux, V. Pont, S. Richard, D. Sighomnou, and J. P. Lacaux (2003), Rainwater chemistry and wet deposition over the equatorial forested ecosystem of Zoétélé (Cameroon), *J. Atmos. Chem.*, *46*, 173–198.

Staudt, A. C., D. J. Jacob, F. Ravetta, J. A. Logan, D. Bachiochi, T. N. Krishnamurti, S. Sandholm, B. Ridley, H. B. Singh, and B. Talbot (2003), Sources and chemistry of nitrogen oxides over the tropical Pacific, *J. Geophys. Res.*, *108*(D2), 8239, doi:10.1029/2002JD002139.

Swap, R. J., T. A. Szuba, M. Garstang, H. J. Annegarn, L. Marufu, and S. J. Piketh (2003), Spatial and temporal assessment of sources contributing to the annual austral spring mid-tropospheric ozone maxima over the tropical South Atlantic, *Glob. Change Biol.*, *9*, 336–345.

Thompson, A. M., K. E. Pickering, D. P. McNamara, M. R. Schoeberl, R. D. Hudson, J. H. Jim, E. V. Browell, V. W. J. H. Kirchhoff, and D. Nganga (1996), Where did tropospheric ozone over southern Africa and the tropical Atlantic come from in October 1992?: Insights from TOMS, GTE TRACE A, and SAFARI 1992, *J. Geophys. Res.*, *101*, 24,251–24,278.

Wang, Y., D. J. Jacob, and J. A. Logan (1998), Global simulation of tropospheric O_3-NO_x-hydrocarbon chemistry: 1. Model formulation, *J. Geophys. Res.*, *103*, 10,713–10,725.

Yevich, R., and J. A. Logan (2003), An assessment of biofuel use and burning of agricultural waste in the developing world, *Global Biogeochem. Cycles*, *17*(4), 1095, doi:10.1029/2002GB001952.

Yienger, J. J., and H. Levy II (1995), Empirical model of global soil-biogenic NO_x emissions, *J. Geophys. Res.*, *100*, 1447–1464.

Ziemke, J. R., and S. Chandra (1999), Seasonal and interannual variabilities in tropical tropospheric ozone, *J. Geophys. Res.*, *104*, 21,425–21,442.

K. Chance and T. P. Kurosu, Harvard-Smithsonian Center for Astrophysics, 60 Garden Street, Cambridge, MA 02138-1516, USA. (kchance@cfa.harvard.edu; tkurosu@cfa.harvard.edu)

C. Galy-Lacaux, Observatoire Midi-Pyrénées, Laboratoire d'Aérologie, UMR CNRS/Université Paul Sabatier 5560, 14 Avenue Edouard Belin, F-31400 Toulouse, France. (llacc@aero.obs-mip.fr)

D. J. Jacob, Division of Engineering and Applied Sciences and Department of Earth and Planetary Sciences, Harvard University, Pierce Hall, 29 Oxford Street, Cambridge, MA 02138, USA. (djacob@fas.harvard.edu)

L. Jaeglé and L. Steinberger, Department of Atmospheric Sciences, University of Washington, Box 351640, Seattle, WA 98195-1640, USA. (jaegle@atmos.washington.edu; llou@atmos.washington.edu)

R. V. Martin, Department of Physics and Atmospheric Science, Dalhousie University, Halifax, Nova Scotia B3H 3J5, Canada. (rvmartin@fizz.phys.dal.ca)

A. I. Modi, Département de Physique, Ecole Normale Supérieure, Université Abdou Moumouny de Niamey, BP 10963 Niger, Africa. (aimod@yahoo.com)

L. Sigha-Nkamdjou, Centre de Recherches Hydrologiques, BP 4110 Yaoundé, Cameroun. (lucsigha@hotmail.com)

V. Yoboué, Laboratoire de Physique de l'Atmosphère, Université de Cocody, BP 582, Abidjan, Ivory Coast, Africa. (yobouev@hotmail.com)

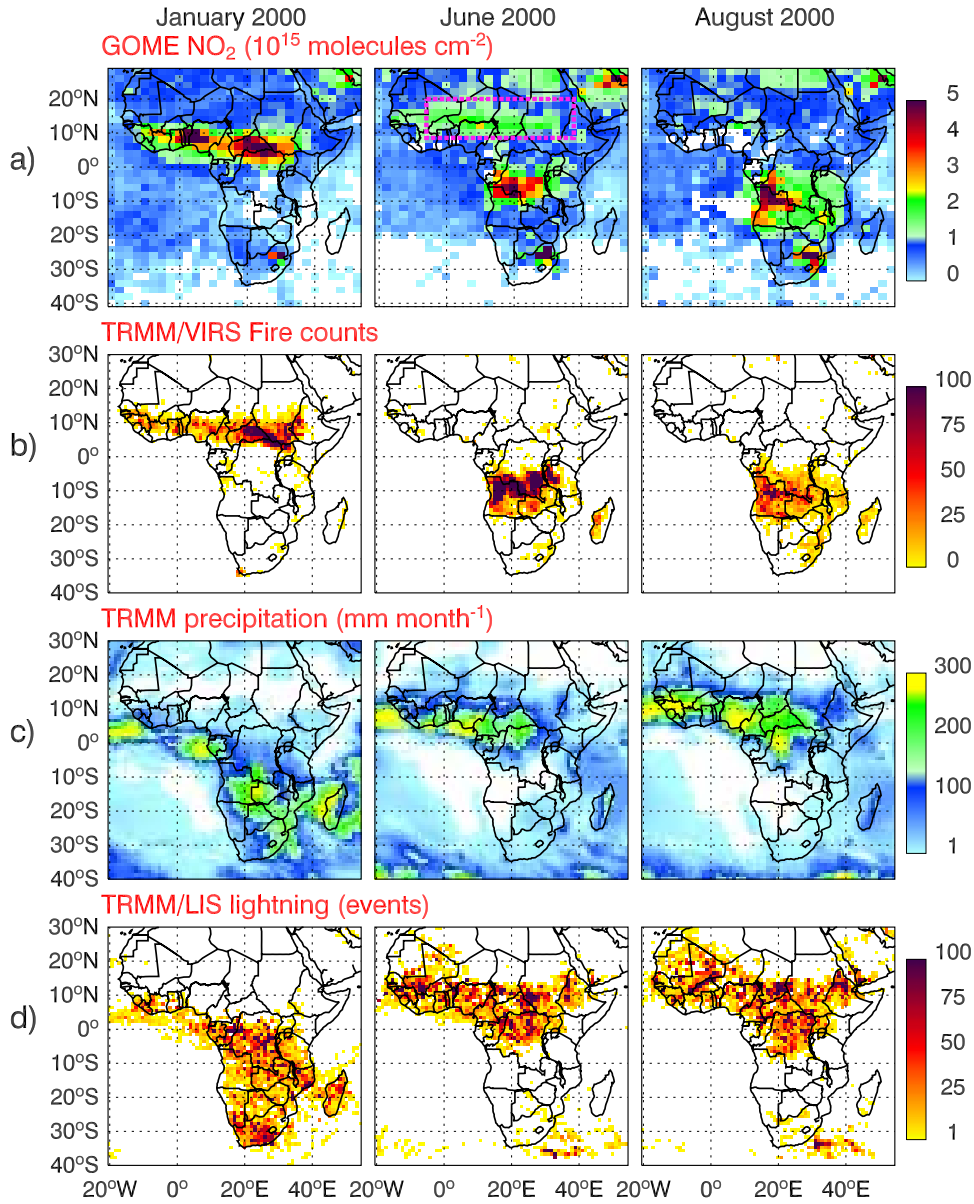

Figure 1. Space-based observations of NO_2 columns, fires, precipitation and lightning over Africa for January, June, and August 2000. (a) Monthly mean GOME NO_2 tropospheric columns in 10^{15} molecules cm^{-2}. (b) Total active fires observed by the Visible and Infrared Scanner (VIRS) on board the TRMM satellite. (c) Monthly precipitation from the TRMM merged analysis in mm $month^{-1}$. (d) Monthly lightning activity from the lightning imaging sensor (LIS) on board TRMM. GOME observations are averaged over a 2° latitude by 2.5° longitude horizontal grid, while all TRMM observations are averaged over a 1° × 1° grid. The NO_2 enhancements over the Sahel region during June are highlighted with a dotted rectangle in the top panel.

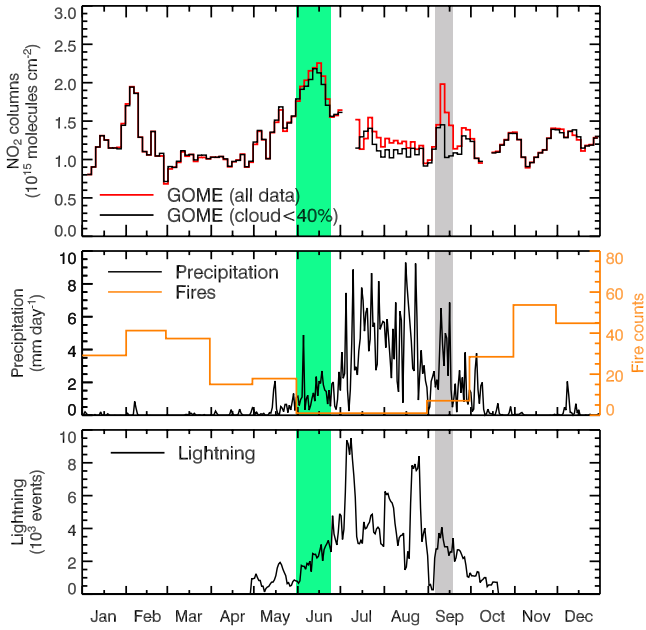

Figure 2. Evolution of NO_2, precipitation and fires over 1.5 million km^2 of the southern Sahel (12–16°N; 0–30°E). (top) Time series of 3-day composite tropospheric GOME NO_2 columns averaged over the southern Sahel. All data (red) as well as cloud-filtered data (black, <40% cloud cover) are shown. A 9-day running average was used to smooth the observations. Gaps indicate 6 days or more without observations. (middle) TRMM daily precipitation (black line) and monthly fire counts (orange line). (bottom) TRMM/LIS lightning events. The green shading indicates the June soil NO_x pulse, while the gray shading shows a later pulse in September (section 3).

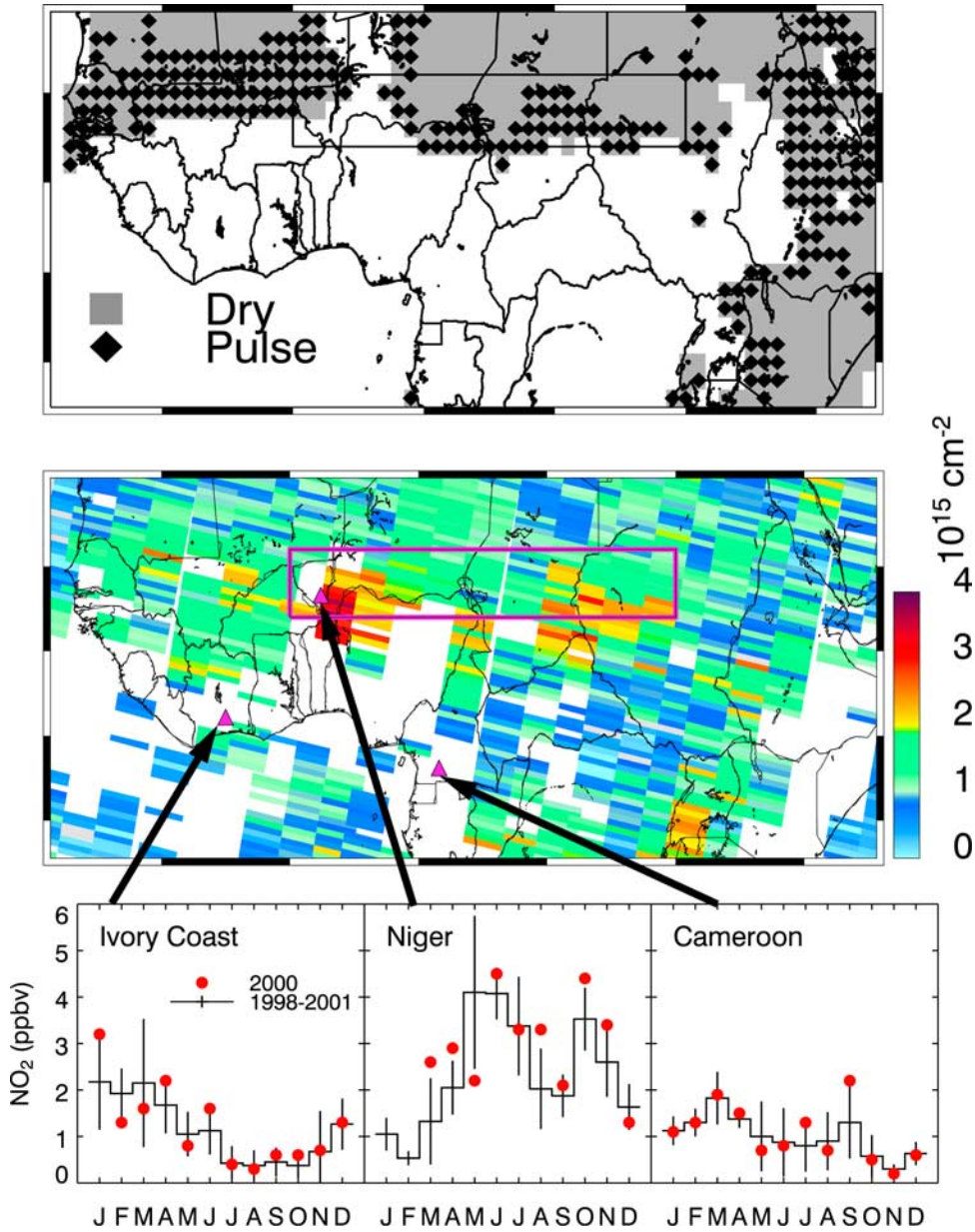

Figure 3. (top) Accumulated rainfall and soil pulsing derived from TRMM daily precipitation for 7–12 June 2000. Gray areas indicate dry soils (accumulated precipitation over the last 14 days <20 mm) and black diamonds correspond to dry soils with recent rainfall occurring over the 7–12 June time period. (middle) Three-day composite map of GOME tropospheric NO_2 columns for 10–12 June 2000. White areas are for cloud cover >40%. The thick rectangle shows the area plotted in Figure 2 (12–16°N; 0–30°E). (bottom) Monthly surface NO_2 measurements from the IDAF network in wet savanna (Lamto, Ivory Coast: 6.1°N, 5.0°W), semiarid savanna (Banizoumbou, Niger: 13.3°N, 2.4°E), and rain forest (Zoétélé, Cameroon: 3.1°N, 11.6°E) sites. Red circles show the 2000 observations, while black lines show the mean (and standard deviations) for 1998–2001.

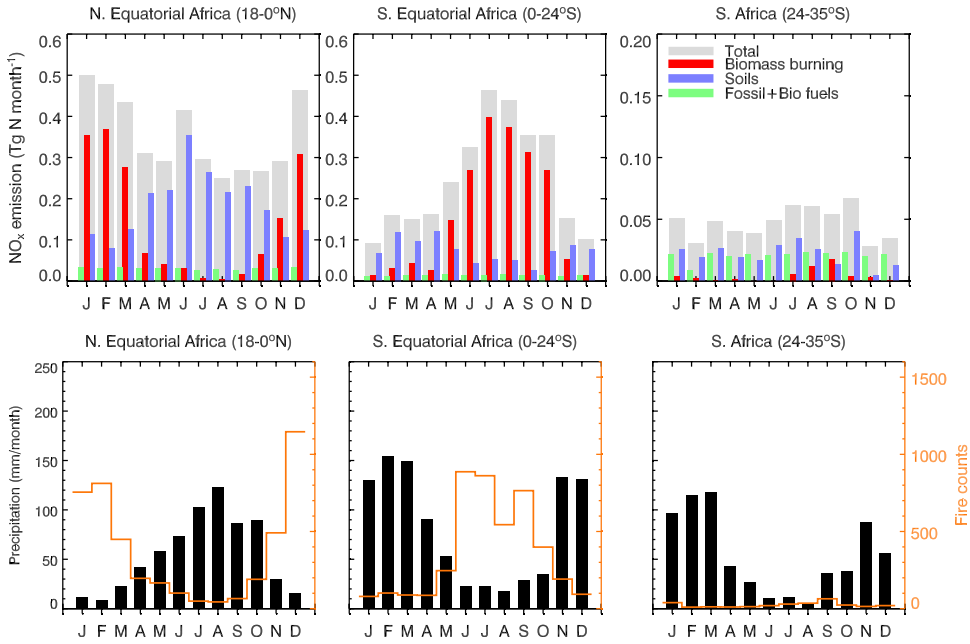

Figure 4. Monthly NO_x emissions, fires and rainfall over north equatorial Africa (18–0°N), south equatorial Africa (0–24°S) and southern Africa (24–35°S) in 2000. (top) Monthly top-down GOME NO_x emissions averaged over each region (gray bars). Note the different scale on the right-most panel. We combine bottom-up estimates of biofuel and fossil fuel NO_x emission inventories with the spatial location of fires to partition emissions between biomass burning (red bars), soil (blue bars), and fossil+biofuel (green bars) sources. (bottom) Seasonal variations in total active fires (solid orange line) and mean precipitation (black bars) observed by TRMM.